Earth Wind as a Possible Exogenous Source of Lunar Surface Hydration

H. Z. Wang[1,2], J. Zhang[1] , Q. Q. Shi[1,2] , Y. Saito[3], A. W. Degeling[1] , I. J. Rae[4] , Q. G. Zong[5], Y. Wei[6] , J. Liu[2] ,
R. L. Guo[7], Z. H. Yao[6], A. M. Tian[1] , X. H. Fu[1], J. Z. Liu[8], Z. C. Ling[1], S. Y. Fu[5], W. J. Sun[9] , S. C. Bai[1], J. Chen[1] ,
S. T. Yao[1] , H. Zhang[6] , W. L. Liu[10], L. D. Xia[1] , Y. Y. Feng[2,11], and Z. Y. Pu[5]

[1] Laboratory of Optical Astronomy and Solar-Terrestrial Environment, School of Space Science and Physics, Institute of Space Sciences, Shandong University,
Weihai, Shandong, 264209, People's Republic of China; zhang_jiang@sdu.edu.cn, sqq@sdu.edu.cn
[2] State Key Laboratory of Space Weather, National Space Science Center (NSSC), Chinese Academy of Sciences, Beijing, People's Republic of China
[3] Institute of Space and Astronautical Science, Japan Aerospace Exploration Agency, Sagamihara, Japan
[4] Department of Maths, Physics and Electrical Engineering, Northumbria University, Newcastle, UK
[5] School of Earth and Space Sciences, Peking University, Beijing, People's Republic of China
[6] Key Laboratory of Earth and Planetary Physics, Institute of Geology and Geophysics, Chinese Academy of Sciences, Beijing, People's Republic of China
[7] Laboratoire de Physique Atmosphérique et Planétaire, STAR Institute, Université de Liège, Liège, Belgium
[8] Center for Lunar and Planetary Sciences, Institute of Geochemistry, Chinese Academy of Sciences, Guiyang, People's Republic of China
[9] Department of Climate and Space Sciences and Engineering, University of Michigan, Ann Arbor, MI, USA
[10] School of Space and Environment, Beihang University, Beijing, People's Republic of China
[11] Joint Research and Development Center of Chinese Science Academy and Shen County, Shandong, China

Abstract

Understanding the sources of lunar water is crucial for studying the history of lunar evolution, as well as the interaction of solar wind with the Moon and other airless bodies. Recent orbital spectral observations revealed that the solar wind is a significant exogenous driver of lunar surficial hydration. However, the solar wind is shielded over a period of 3–5 days per month as the Moon passes through the Earth's magnetosphere, during which a significant loss of hydration is expected. Here we report the temporal and spatial distribution of polar surficial OH/H_2O abundance, using Chandrayaan-1 Moon Mineralogy Mapper (M^3) data, which covers the regions inside/outside the Earth's magnetosphere. The data shows that polar surficial OH/H_2O abundance increases with latitude, and that the probability of polar surficial OH/H_2O abundance remains at the same level when in the solar wind and in the magnetosphere by controlling latitude, composition, and lunar local time. This indicates that the OH/H_2O abundance in the polar regions may be saturated, or supplemented from other possible sources, such as Earth wind (particles from the magnetosphere, distinct from the solar wind), which may compensate for thermal diffusion losses while the Moon lies within the Earth's magnetosphere. This work provides some clues for studies of planet–moon systems, whereby the planetary wind serves as a bridge connecting the planet with its moons.

1. Introduction

Understanding the sources and formation processes of lunar water provides important information on the origin and evolution of the Moon (and by extension, other airless planetary bodies), including magmatic evolution, bombardment history, and solar wind–surface interactions. Recent orbital observations and laboratory analyses have revealed a "wet" Moon with various forms of lunar water (Saal et al. 2008; Clark 2009; Pieters et al. 2009; Sunshine et al. 2009; Boyce et al. 2010; Colaprete et al. 2010; Gladstone et al. 2010; Greenwood et al. 2011; Hauri et al. 2011; Hui et al. 2013). These forms of water have been proposed to come from both indigenous and exogenous sources, including the lunar interior, comets, asteroids, the solar wind, and Earth's magnetosphere (Watson et al. 1961; Arnold 1979; Starukhina & Shkuratov 2000).

Evidence of water from the lunar interior was found by laboratory analyses of lunar samples, such as pyroclastic glasses, lunar melt inclusions, apatite grains, and anorthosites (Saal et al. 2008; McCubbin et al. 2010; Hauri et al. 2011; Hui et al. 2013; Saal et al. 2013), and was also found in pyroclastic deposits by orbital spectral observation (Milliken & Li 2017). In contrast, examples of exogenous origins include the episodic delivery of water to the Moon from meteoroids and comets (Keays et al. 1970), resulting in deuterium/hydrogen (D/H) values that differ

from lunar interior sources (Greenwood et al. 2011; Barnes et al. 2016).

Solar wind protons are considered to be another exogenous source of water (Watson et al. 1961; Zeller et al. 1966; Starukhina & Shkuratov 2000; Clark 2009; Pieters et al. 2009; Sunshine et al. 2009; Kramer et al. 2011; McCord et al. 2011; Hendrix et al. 2012; Farrell et al. 2015; Li & Milliken 2017; Wöhler et al. 2017; Bandfield et al. 2018). Surface water abundance has been found to exhibit diurnal variations, which is interpreted as indicating a dynamic balance between a continuous source from the solar wind, and loss processes dependent on solar illumination and surface temperature (Clark 2009; Pieters et al. 2009; Sunshine et al. 2009; McCord et al. 2011; Farrell et al. 2015; Li & Milliken 2017; Wöhler et al. 2017). Lunar sample analyses and laboratory ion irradiation experiments provide further evidence that solar wind protons provide an exogenous source (Djouadi et al. 2011; Ichimura et al. 2012; Liu et al. 2012; Schaible & Baragiola 2014; Zhu et al. 2019). The interpretation in these studies is that lunar water is generated by solar wind proton implantation into the uppermost surface of lunar mineral grains, either forming OH bonds (Zeller et al. 1966; Starukhina & Shkuratov 2000), or generating molecular water via a combination of other processes (Blanford et al. 1985; Zhu et al. 2019).

During about three-quarters of the lunar orbit, the Moon is immersed in solar wind, which provides a predominant proton
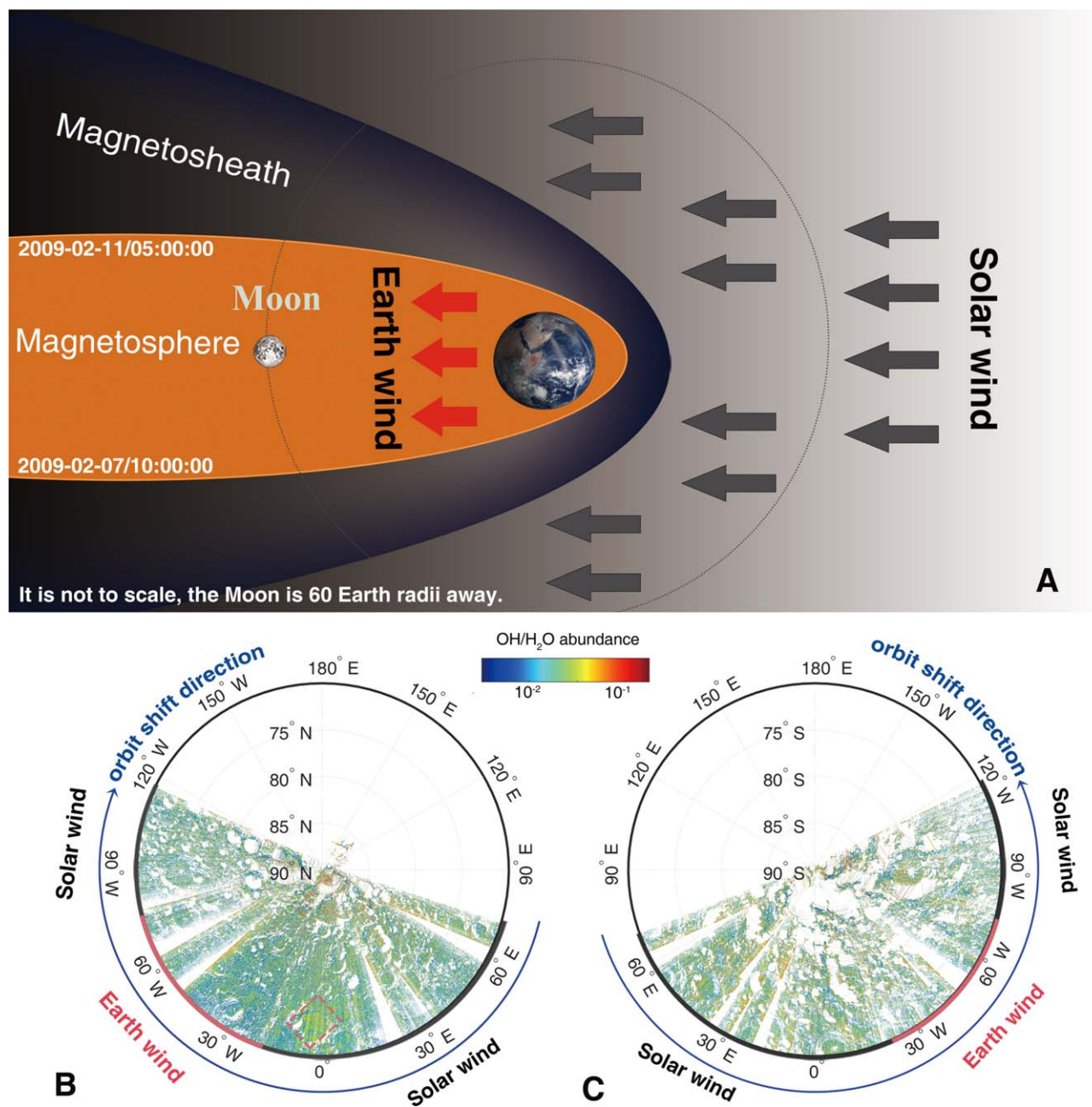
Figure 1. (A) Lunar orbit in a lunation, indicating that for 3–5 days of every lunation, the Moon lies within the Earth's magnetosphere, shielded from the solar wind. (B-North C-South) Overview of lunar OH/H_2O abundance (represented here by strength of 2.8 μm absorption feature) in the polar regions, derived from the M^3 observations from 2009 January 26 to 2009 February 23. There is no data in the blank area. Red and black bars mark the duration of the Moon's exposure to Earth wind and solar wind, respectively. The blue arrow indicates the M^3 orbital shift direction. The red rectangle indicates the Goldschmidt crater, in which lunar OH/H_2O abundance is anomalously high due to its material composition.

flux at ~1 keV, along with 1%–5% alpha particles and other heavy ions (Hundhausen 1970), depending on solar wind speed, heliographic latitude, and solar cycle (Kasper et al. 2007). During the remaining 3–5 days of every lunation, the Moon lies within the Earth's magnetosphere (Figure 1(A)), where it is shielded from most of the solar wind protons. In the absence of other hydrogen sources, a decrease in surface hydration would be expected, due to loss processes such as thermal diffusion and photodissociation (Arnold 1979; Starukhina & Shkuratov 2000). However, the Earth's magnetosphere is not empty; it is occupied by the Earth wind, whose ion constituents and energies are different from those of solar wind. The particle species in the Earth wind consist of both solar wind and terrestrial species (i.e., H^+, He^+, O^+, N_2^+, NO^+, O_2^+) (Christon et al. 1994; Fu et al. 2001; Seki et al. 2001; Zong et al. 2001; Hasegawa et al. 2004; Shi et al. 2013; Wei et al. 2014; Poppe et al. 2016). Particle fluxes are typically several times lower than those of solar wind (Lin et al. 1995); however, the particle energy distribution is significantly broader. Therefore, from the standpoint of both composition and energy, the Earth wind is not simply deflected solar wind.

Ions from the Earth wind have been detected in the vicinity of the Moon (Terada et al. 2017). Harada et al. (2014) reported that backscattered hydrogen energetic neutral atom (ENA) flux

from the Moon in the Earth's magnetosphere plasma sheet is roughly of the same order of magnitude as that of solar wind, which suggests that a significant amount of Earth wind can reach the Moon. Therefore, it is worth studying whether these ions can contribute to lunar surface hydration as an exogenous source, similarly to solar wind.

Recently, (Cho et al. 2018; Li et al. 2018b) have shown, based on selected low latitude (0–10 degree) areas, that lunar surficial water can decrease when the Moon moves into the Earth's magnetosphere, and proposed that the lunar surface may be shielded from the solar wind by the magnetosphere. In their study, cases at higher latitudes were not covered, and the potential for Earth wind as a source of lunar water was not considered. It has been shown, however, that at high latitudes on the lunar surface, the thermal distribution of magnetosphere plasmas can provide hydrogen atoms to the lunar regolith (Starukhina & Shkuratov 2000). This begs the question, which processes are dominant from low to high latitudes when the Moon is within or outside the Earth's magnetosphere?

In this work, in order to examine whether Earth wind could contribute to lunar surficial water when the Moon is in the Earth's magnetosphere, we study the spatial distribution (as a function of latitude) and temporal variations (inside and outside of the magnetosphere) of lunar water at high latitudes, based on the Chandrayaan-1 Moon Mineralogy Mapper (M^3) data, comparing intervals when the Moon lies inside/outside the magnetosphere.

2. Data and Methods

(1) Determining the location of the Moon (relative to Earth's magnetotail) using magnetic field and plasma data from the Kaguya mission.

The Kaguya mission was a lunar polar orbiter at an altitude of ∼30 to 100 km, launched on 2007 September 14, which crashed on the lunar surface on 2009 June 10. Kaguya's observations during its mission had an observation period simultaneous with that of the Chandrayaan-1 mission. We use the plasma and magnetic field data from the Magnetic field and Plasma experiment (MAP) instrument (Saito et al. 2008, 2010; Tsunakawa et al. 2010) on board the Kaguya spacecraft to determine time intervals in which the Moon was in the Earth's magnetosphere during a lunation from 2009 January 26 to 2009 February 23.

(2) Mapping OH/H_2O abundance based on M^3 spectra before, during, and after transiting the Earth's magnetosphere.

The M^3 imaging spectrometer on board the Chandrayaan-1 mission measures reflected solar light from the lunar surface, covering visible and near-infrared wavelengths between ∼460 nm and 3000 nm. This spectral range includes absorption features near 2.8–3 μm caused by OH/H_2O (Pieters et al. 2009). The M^3 is a "push-broom" imaging spectrometer, operated in a circular polar orbit, and obtained data at a spatial resolution of 140 m/pixel in Global mode from its nominal 100 km orbit.

We selected the M^3 data within a lunation from 2009 January 26 to 2009 February 23, while the optical period is OP1B (defined as an approximate 3 month time span, when the solar zenith angle at the lit-side equatorial node of the orbit was less than 45°) in cold thermal operating conditions (Boardman et al. 2011). A list of M^3 data strips are shown in Table A1 in the Appendix. During this time interval the Moon stayed in the Earth's magnetosphere for several days around 2009 February 9 (the full moon period). Lunar near-infrared (NIR) reflectance spectra are affected by the

thermal emission radiation at wavelengths beyond 2 μm, particularly those obtained at low latitudes (Li & Milliken 2016). While the existing thermal correction models give rise to different results (Li & Milliken 2017; Wöhler et al. 2017; Bandfield et al. 2018), in order to reduce any uncertainties introduced by thermal correction models, only the polar regions at latitudes above 70° are studied in this work, due to their lower temperatures (average ∼280 K) (Pieters et al. 2009), in which thermal residuals are suppressed in the first-order thermal corrections of the M^3 data. Any "bad" pixels with lower and flat reflectance spectra are removed, based on their wavelength-reflectance 2D histogram. We then calculate the relative band depth H around 2.8 μm as an indicator of lunar surface OH/H_2O abundance,

$$H = 1 - \frac{R_b}{R_c}$$

where R_b is the average reflectance over channels of OH/H_2O absorption features between 2896 and 2936 nm, and R_c is the average reflectance over channels of 2617, 2657, and 2697 nm, representing the reflectance continuum (Pieters et al. 2009).

(3) Controlling factors affecting OH/H_2O abundance.

Previous studies suggest that lunar surficial water abundance is dependent on various factors, such as latitude (Pieters et al. 2009; McCord et al. 2011; Li & Milliken 2017), lunar local time (Sunshine et al. 2009; Li & Milliken 2017; Wöhler et al. 2017), and surface composition (Cheek et al. 2011). In order to study the effect of variations in the sources of lunar water, we need to control other contributing factors. The latitude is taken from the M^3 data, and the local time of the M^3 data is calculated from the observation time and longitude using the SPICE Toolkit package developed by the NASA PDS NAIF node (Acton 1996).

We use FeO abundance obtained by the Lunar Prospector (LP) Gamma Ray Spectrometer to locate compositionally similar regions, as this is the only data set to completely cover the polar regions, and is available at a spatial resolution of 0.5 degree per pixel (Lawrence et al. 2002).

(4) Averaging the differential ion energy flux distribution before /during /after transiting Earth's magnetosphere, using ARTEMIS data.

Having controlled the latitude, local time, and composition that could affect OH/H_2O abundance, we then use ARTEMIS data to study the relationship between lunar surface hydration and the incident solar/Earth wind ion energy flux.

The ARTEMIS mission consists of a pair of identically instrumented spacecraft in orbit around the Moon since mid-2011 (Angelopoulos 2011; Sibeck et al. 2011). Both probes measure the in situ low-energy ion (up to 25 keV) and electron (up to 30 keV) distributions with an electrostatic analyzer (ESA) (McFadden et al. 2008). In the computation, we excluded those periods when the probes traversed the lunar nightside, in order to avoid the influence of the lunar wake, in which the solar wind is shielded.

3. Observations

Overview maps of lunar surficial hydration at the polar regions, derived from the M^3 observations from 2009 January 26 to 2009 February 23, are presented in Figures 1(B)–(C). The interval when the Moon is in the Earth's magnetosphere, determined by the Kaguya MAP data (Saito et al. 2008, 2010; Tsunakawa et al. 2010) on 2009 February, is from 2009 February 07/10:00 to 2009 February 11/05:00 (3.8 days). In
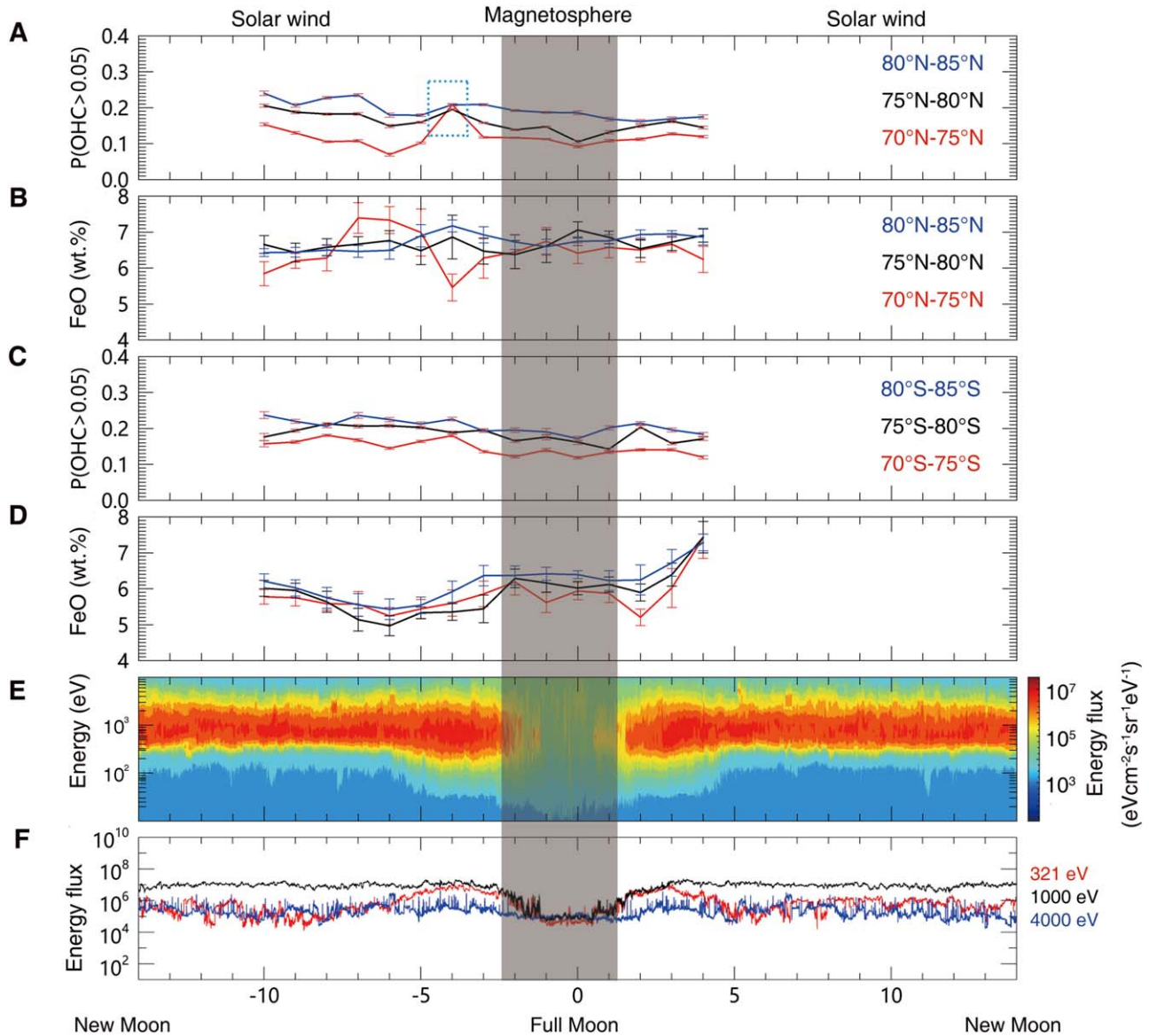
Figure 2. OH/H$_2$O and FeO abundances at lunar polar regions during a lunation from 2009 January 26 to 2009 February 23, and ion energy flux distribution averaged over five-year observations. (A–D) The probability of 2.8 μm absorption depth between 0.05 and 0.20 represents the OH/H$_2$O abundance level and mean value of FeO represents the composition abundance level for each 5° latitude and 24 Earth hours bin. The zero epoch in the top four panels indicates full moon time during the M^3 observation. The error in figures A and C is calculated by $\varepsilon = \frac{n}{N} * \left(\frac{\sqrt{n}}{n} + \frac{\sqrt{N}}{N} \right)$, where n is the number of pixels with an absorption depth greater than 0.05, and N is the number of pixels with an absorption depth less than 0.2 in each bin, such that the occurrence rate for each bin is $N_0 = n/N$. The Poisson error for event number n is $\sqrt{n}$. Similarly, the Poisson error for event number N is $\sqrt{N}$. Using the propagation of error analysis according to average deviations, the uncertainty of the normalized value for each bin is $\Delta N_0 = N_0 \sqrt{\left(\frac{\sqrt{n}}{n} \right)^2 + \left(\frac{\sqrt{N}}{N} \right)^2}$ $(2 \frac{\sqrt{n}}{n} * \frac{\sqrt{N}}{N}$ close to zero). The error bar shown in the figure is scaled by a factor of 10. The error in figures B and D is the standard deviation. The anomaly indicated by the blue dashed line rectangle is caused by highland materials within the Goldschmidt crater. The gray shaded area marks the duration of the Moon's location in the Earth's magnetosphere, as determined by the Kaguya observations. (E–F) A superposed epoch analysis of (E) ion spectrogram and (F) ion energy flux $\sim$321 eV(red), $\sim$1 keV(black), and $\sim$4 keV(blue) as a function of lunar phase, using the five-year ARTEMIS data from 2011 September to 2016 October, where the zero epoch in the two bottom panels indicates the full moon times, over five years of ARTEMIS observations.

general, we find that there are no significant differences in the probability of OH/H$_2$O abundance for intervals when the Moon is located in the Earth's magnetosphere and in the solar wind. More quantitative comparison results are shown in Figure 2 and Table A2 in the Appendix. It should be noted that the M^3 orbit shifted in longitude, as indicated by the blue arrow in Figures 1(B)–(C) and A1 in the Appendix. In Figures 1(B)–(C), the red and black bars mark the duration of the Moon's location in the Earth wind and the solar wind, respectively. In Figure A1 in the Appendix, the lunar surficial hydration

before/during/after transiting through the Earth's magnetotail are shown separately in latitude–longitude grid maps. As shown by Figures 1(B)–(C) and Figure A1 in the Appendix, the M^3 observation covered different regions when in the solar wind and Earth wind. Thus, as mentioned in Section 2, we need to compare the OH/H$_2$O abundance in similar regions when the Moon was in the solar wind or Earth wind by controlling the surface composition, latitude, and local time.

Firstly, in order to show more clearly when the Moon was in the magnetotail, we convert the M^3 observation time into lunar

day (the 28 days before and after the full moon time), considering the fact that the average full moon position is in the center of the magnetotail, where the Sun, Earth, and Moon are roughly aligned. Thus, the full moon period, around which the Moon was within the magnetosphere, are taken as the zero epoch, with the previous and next new moon times corresponding to the left- and right-hand sides. Around the full moon period on February 9, considering the solar wind Vy to be $\sim 10\,km\,s^{-1}$, $Vx \sim -325\,km\,s^{-1}$ (Omni data) and the revolution speed of the Earth around the Sun to be $30\,km\,s^{-1}$, the magnetotail axis deviates ~ 7 degrees westward. This leads to ~ 0.5 day right shift of the full moon position (GSE $Y = 0$) from the center of magnetotail in Figure 2. A sudden and large amplitude solar wind deflection can indeed change the location of the magnetopause. For example, during an event studied by Shang et al. (2020), it was shown that the magnetotail was pushed aside, exposing the full moon to the solar wind, by an appreciable solar wind deflection ($Vy/Vx \sim 200/750\,km\,s^{-1}$). However, we have checked the solar wind conditions during the lunation interval studied here, and did not find any evidence of extreme solar wind deflections, as reported by Shang et al. (2020). Longitudinal variation with lunar day, taken from the M^3 data, are shown in Figure A2 in the Appendix. It is likely that the OH/H_2O abundance may be saturated at high latitude ($85°$–$90°$), given the very low temperature in this region. Therefore, we only investigated the possibility of OH/H_2O abundance varying with lunar day at latitudes from $70°$–$85°$. We then divided the data into three groups as a function of latitude ($70°$–$75°$, $75°$–$80°$, and $80°$–$85°$) to show the spatial distribution, using the lunar day as the horizontal axis in Figure 2 to show the temporal variation. In so doing, we quantitatively show the spatial and temporal variations of lunar surface hydration, particularly those inside/outside the Earth's magnetosphere, using the epoch analysis in Figure 2.

In Figures 2(A) and (C), the OH/H_2O data points are binned into $5°$ latitude and 24 Earth hour intervals. The histogram statistics for the absorption depth around $2.8\,\mu m$ at high latitudes ($70°$–$90°$) is shown as a broad distribution in Figure A3 in the Appendix. This figure indicates that it is not useful to describe this data distribution using only averaged values; we therefore calculate the probability of OH/H_2O abundance above a particular value (0.05) to represent the OH/H_2O abundance level. As shown by Figures 1(B–C) and 2 (A and C), the lunar surface OH/H_2O abundance increases with latitude toward the polar regions, which is consistent with previous studies (Pieters et al. 2009; McCord et al. 2011; Li & Milliken 2017). The anomaly indicated by the rectangle in Figure 2(A) is caused by highland materials within the Goldschmidt crater (Pieters et al. 2009). Previous studies have suggested lunar surface hydration dependence with composition (Pieters et al. 2009); thus we use the FeO map derived from the Lunar Prospector Gamma Ray Spectrometer (Lawrence et al. 2002) in the assessment of lunar hydration variation inside/outside Earth's magnetosphere. The average value of FeO data in each bin is shown in Figures 2(B) and (D). By analyzing these binned data along with the lunar day at different latitude ranges, an overview of the spatial distribution (latitude $70°$–$90°$) and temporal variation (before/during/after transiting through the magnetotail) of lunar surficial hydration can be compiled. However, the FeO abundance for the regions covered by the M^3 data in the Earth's magnetosphere does not vary significantly. Specifically, the FeO abundance in the M^3

observed regions for all latitudes where the Moon was about to enter the magnetosphere does not show a significant difference (<0.68 wt.%, the FeO difference when the Moon was about to enter the magnetosphere (the day before the magnetosphere) and when the Moon about to exit the magnetosphere (the last day in the magnetosphere) compared to the regions where the Moon was about to exit the magnetosphere. In addition, time of day effects can be excluded, since the M^3 observations were generally conducted at the same local time in this lunation (shown in Table A3 in the Appendix). It is found that the probability of lunar OH/H_2O abundance when inside the Earth's magnetosphere (gray shading in Figures 2(A) and C) remains at nearly the same level as when the Moon is exposed to solar wind, even taking into consideration the effects of latitude, composition, and time of day. This can be further quantitatively analyzed by calculating the relative frequency (Figure A4 in the Appendix) of OH/H_2O abundance (the ratio of the number of data points in each histogram bin to the total number of data points in the histogram), and the quartile values (Table A2 in the Appendix) at the northern and southern polar regions, when exposed to solar wind or Earth wind at different latitudes, by controlling FeO abundance (6 wt.% $\sim$ 7 wt.%) and lunar local time (8 am $\sim$ 9 am). We find that most of the relative differences in the quartile values between the OH/H_2O abundance in the solar wind and in the Earth wind fall within $\pm 10\%$, indicating that OH/H_2O abundance in solar wind and Earth wind can be considered to be at the same level.

Finally, after controlling the factors mentioned above, we should consider another cause of variation in lunar hydration due to proton sources. It is well known that when the Moon passes through the Earth's magnetosphere, solar wind incident on the Moon vanishes. To investigate the correlation between lunar surface hydration and the incident ion energy flux, we computed the average differential ion energy spectrum and the $\sim 1\,keV$ (typical hydrogen ion energy in the solar wind), $\sim 321\,eV$, and $\sim 4\,keV$ mean values of ion energy flux incident on the Moon as a function of lunar phase (where 0 defines "full moon" and $-14/14$ indicates "new moon") as shown in Figure 2 E–F. We find that the incoming $\sim 1\,keV$ ion flux when within the Earth's magnetosphere is about two orders of magnitude lower than that found during exposure to solar wind (Figures 2(E)–(F) and Figure 4).

4. Discussion

4.1. Possible Mechanisms for Unchanged Polar Surficial Hydration Across Magnetotail

As mentioned in the previous sections, solar wind is thought to be a primary source for lunar global surficial OH/H_2O (Arnold 1979; Pieters et al. 2009; Sunshine et al. 2009). On the other hand, loss mechanisms for lunar surficial water include recombination desorption (Jones et al. 2018), thermal diffusion (Starukhina & Shkuratov 2000; Farrell et al. 2017), sputtering (Barghouty et al. 2011), photodissociation (Arnold 1979), and meteoroid impact (Langevin & Arnold 1977; Zhu et al. 2019), with recombination desorption and thermal diffusion both being dependent on temperature (Farrell et al. 2017; Jones et al. 2018) (see Table A4 in the Appendix for details on production and loss processes). The above results have shown that the proton flux at $\sim 1\,keV$ in the Earth's magnetosphere is two orders lower than that in the solar wind. However, based on our observations, the probability of OH/H_2O abundance at the polar regions showed no
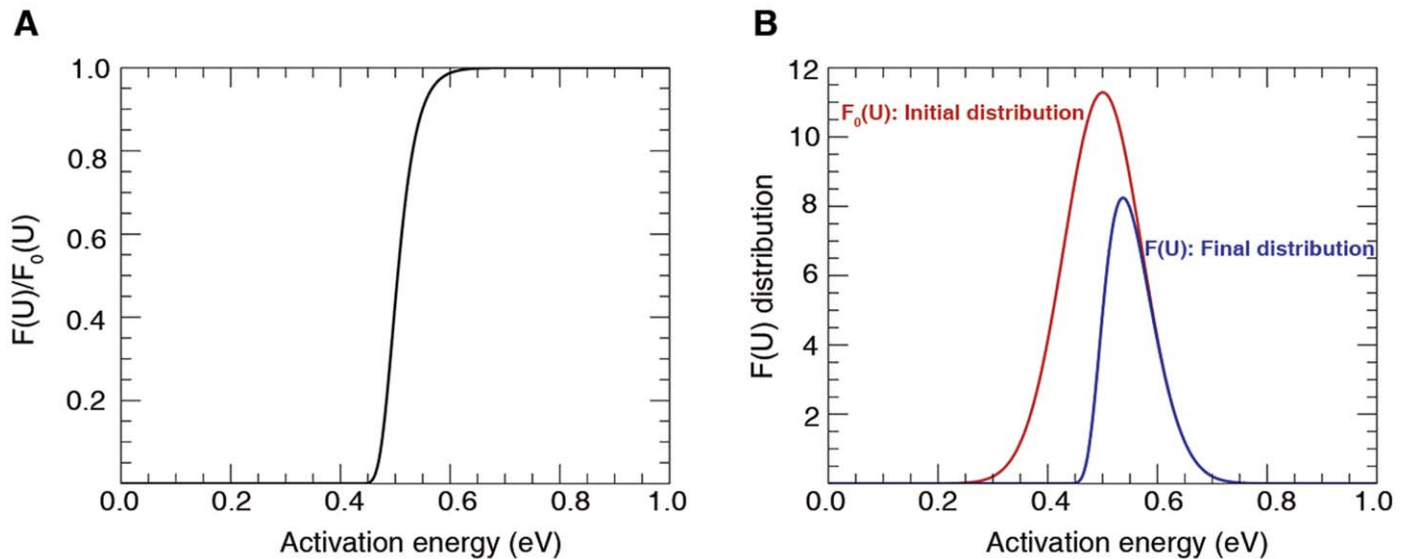
Figure 3. Temporal evolution of implanted hydrogen distribution with activation energy when the sources are turned off. The results are calculated using the model described in (Farrell et al. 2017), with $T = 280$ K and duration $\Delta t = 3.8$ days. (A) The ratio between the final and initial H distribution. The implanted H with activation energy above ~0.7 eV is retained, while those with U < 0.65 eV tend to escape. (B) Initial (red) and final H (blue) distributions.

significant reduction when the Moon was in the Earth's magnetotail. There are several possible mechanisms to explain these observations, including: 1) The OH/H_2O is possibly saturated when exposed to solar wind, while the loss processes are too weak to cause notable OH/H_2O variation within the magnetotail, due to lower temperatures toward the polar regions (Jones et al. 2018). In this case, the abundance of OH/H_2O at polar regions would not be affected by magnetotail shielding; 2) The OH/H_2O suffers larger losses due to thermal diffusion at lower latitudes of the polar regions (Farrell et al. 2017), which means that there should be other possible sources that can compensate for OH/H_2O abundance other than the solar wind, such as water reservoirs in permanently shadowed regions (Farrell et al. 2013), carbonaceous chondrite-like impactor-derived water residing in impact melts and projectile survivors (Daly & Schultz 2018), and Earth wind (Starukhina & Shkuratov 2000).

In terms of the first situation, which can be explained using the kinetic and mechanistic chemical Model developed by Jones et al. (2018), the M-OH formed via solar wind implantation is chemically bound for its high activation energy, and OH is the mobile molecule that produces exospheric water via second-order recombinative desorption. At polar regions (latitude 75°–90°), the temperature is low enough that the loss of OH/H_2O due to this recombination desorption process may be irrelevant. If so, the OH/H_2O will stay stable and accumulate until it saturates at polar regions (Jones et al. 2018). In this case, OH/H_2O abundance will not be affected by the absence of solar wind protons due to magnetotail shielding.

Soil grains on the lunar surface irradiated by solar wind protons can produce vacancies at crystal lattice sites, leading to the formation of amorphous rims (Keller & McKay 1997). In the model based on the diffusion-mediated transport of chemically trapped implanted hydrogen (Farrell et al. 2017; Tucker et al. 2019), the implanted solar wind protons can be hindered and dwell with oxygen atoms within mineral grains, forming permanent or metastable OH bonds which depend on their distribution of activation energy (Farrell et al. 2017; Tucker et al. 2019). This model is based on the experimental study by Fink et al. (1995). The solar wind hydrogen retention time depends on

both activation energy and lunar surface temperature; the implanted hydrogen would effectively dwell within lunar minerals in cold regions (Starukhina 2001, 2012; Farrell et al. 2015). The OH bonds have a Gaussian distribution of activation energy, and below a certain temperature, the OH is stable and permanent with a subset of trapped H atoms with high activation energies; Meanwhile, OH bound with low activation energies is metastable, and will outgas quickly.

In this case, at the colder (i.e., higher) latitudes of polar regions, H retention time exceeds a lunation, due to lower thermal diffusion loss (Farrell et al. 2017). The OH/H_2O will also accumulate until saturation at polar regions, and will not be affected by the absence of solar wind protons caused by magnetotail shielding, which similarly to the first situation. However, at lower latitudes in polar regions, e.g., 70°–75°, where the temperature is ~280 K on average (Li & Milliken 2016; Milliken & Li 2017), the retained H will decrease, with diffusive losses caused by thermal diffusion in these conditions (Farrell et al. 2017). When the Moon passes through the Earth's magnetosphere, the bulk of the solar wind is shielded. If there were no other sources providing additional OH/H_2O at the same time, its abundance should decrease with time due to the diffusive losses caused by thermal diffusion. The retained hydrogen in lunar minerals can be calculated using the analytical approach given by Farrell et al. (2017): 1) The M^3 temperature data, provided by Li & Milliken (2016); Milliken & Li (2017) were used in our residence time calculation, where the temperature measured around 270–300 K (~280 K on average) between 70° N and 75° N when the Moon was about to exit the Earth's magnetosphere; 2) the length of time over which the surface is warmed in the calculation is 3.8 days (determined by the Kaguya MAP measurements); 3) the diffusion coefficient is given by laboratory experiments by Fink et al. (1995); 4) the activation energy distribution is taken from Farrell et al. 2017 and Tucker et al. 2019, whose modeling results are consistent with the M^3 observations. As shown in Figure 3(A), the implanted H with activation energy above ~0.7 eV is retained, while those with activation energy U < 0.65 eV tend to escape, resulting in an overall reduction in retained H to 46% of the initially implanted

level (Figure 3(B)). In addition, as shown by the results from the (Farrell et al. 2017) model, the hydrogen would diffuse out of lunar minerals when the temperature is above 200 K, and be retained when below 200 K. Hence, those regions with lower temperatures at higher latitude would possibly be saturated, and the lack of variation in hydration during magnetotail passage could be explained by long residence times at low temperatures. However, if we take into account surface loss processes other than diffusion, such as meteorite impact (Hurley et al. 2017) and photodissociation (Watson et al. 1961; Arnold 1979), the surface hydration may not be saturated by 200 K. This suggests that when the solar wind is shut off, saturation is unlikely at latitudes at least between 70° and 80° where the temperature is above 200 K. Therefore, any observed reduction in solar wind proton flux while the Moon lies within the Earth's magnetosphere should produce a significant reduction in surface water. The lack of such a reduction in surface OH/H_2O in the observations may imply that possible sources other than solar wind might exist, e.g., large water reservoirs at the lunar polar regions, carbonaceous chondrite-like impactor-derived water residing in impact melts and projectile survivors (Daly & Schultz 2018), and/or the Earth wind.

Firstly, if there are very large water reservoirs at the cold polar trap regions, the surface OH/H_2O would hardly be affected by the lack of solar wind over a few days, and even then, any small changes would be attributed to migration/ diffusion of the hydrated molecules. For instance, a high abundance of water was found within the plume impact on Cabeus crater by the Lunar Crater Observation and Sensing Satellite (LCROSS) mission (Colaprete et al. 2010), and orbital spectral albedo observations suggested that the water ice layers in these craters were due to the extremely cold temperature (Gladstone et al. 2010; Li et al. 2018a). However, the only significant known reservoirs are highly localized and sparsely scattered, occurring within permanently shadowed regions inside craters. Polar water could transport from reservoirs over a wider region and lower latitudes via micrometeoroid impact vaporization and solar wind sputtering. However, the sparsity of these sources is such that the source intensity from this process is too low to fully account for the infrared (IR) observations (Farrell et al. 2013). Another possible reservoir might be globally distributed deeper volatiles in the lunar regolith (Livengood et al. 2015), which may also explain our observations. In addition, water from carbonaceous chondrite-like impactors, trapped in impact melts and later released by meteorite gardening, could also provide a source for the cold polar traps on the Moon (Daly & Schultz 2018). Although we cannot completely rule out these possibilities, recent observations of magnetic anomalies (Kramer et al. 2011; Li & Garrick-Bethell 2019) found some significance of exogenous sources such as solar wind, which motivate us to consider another explanation related to exogenous sources.

4.2. Earth Wind as a Possible Exogenous Source

Alternatively, particles from the Earth's magnetosphere could be an additional source in the absence of solar wind. Starukhina & Shkuratov (2000) proposed that the Earth's magnetosphere can provide hydrogen atoms for the lunar regolith in permanently shadowed regions because of the thermal distribution of magnetosphere plasmas; Lucey (2009) also suggested that ions from the Earth's magnetosphere could be a source of lunar volatiles in polar cold traps. However, to the best of the authors' knowledge, there are no studies to date that have discussed the Earth's magnetotail particles as an additional source for global lunar hydration. This is despite the finding of Harada et al. (2014) that backscattered hydrogen energetic neutral atom (ENA) flux from the Moon in the Earth's magnetosphere plasma sheet is roughly of the same order of magnitude as that in the solar wind, which suggests that a significant amount of Earth wind can reach the Moon. Beam-like solar wind flux reaching the lunar surface decreases with increasing latitude (Hemingway et al. 2015), but the thermal distribution of magnetosphere plasma can provide hydrogen atoms for the lunar regolith at high latitudes (Starukhina & Shkuratov 2000).

Earth Wind is clearly different from solar wind in both energy and composition. Solar wind mainly contains proton flux at ~ 1 keV, with $1\% \sim 5\%$ comprising alpha particles and other heavy particles, while the Earth wind's composition is very dynamic, containing protons, oxygen, nitrogen ions, etc., at different energies. The plasma in the Earth's magnetotail comprises species from two sources: solar wind plasma, which has been accelerated/heated, and cold plasma outflowing from the earth's upper atmosphere/ionosphere. The magnetotail consists of several different regions, such as the plasma sheet (with ion energy ten times higher than that of the typical solar wind) and lobes mainly containing very cold ions from the Earth's upper atmosphere. In Figure 4, we plot differential proton energy fluxes in solar wind and in Earth wind, using the averaged 5 yr ARTEMIS ESA data. Two groups of intersection points are obtained: the lower energy intersection points around 325–430 eV, and the higher intersection around 2.5–4 keV. The average differential proton energy fluxes with energy values less than 325 eV or greater than 4 keV are greater in Earth wind than in solar wind; and those with energy values between 430 eV and 2.5 keV are greater in solar wind.

The different variations of lunar OH/H_2O abundance inside/ outside of the Earth's magnetosphere at different latitudes may be related to both formation and loss processes. As mentioned above, the thermal diffusion loss rate is higher at lower latitudes because of its higher temperature (Farrell et al. 2017). However, our calculation above shows that the loss rate at high latitudes is not very low, and that therefore some formation process must be involved to maintain the same level of water abundance as in solar wind. In solar wind, the protons have a beam-like velocity distribution with a narrow thermal spread centered at the solar wind bulk velocity. However, the protons in the Earth's magnetosphere, particularly those in the plasma sheet, have a broad velocity distribution with a wide thermal spread (Feldman et al. 2001; Harada et al. 2014) (see Figure 4) and a larger portion can reach the lunar surface (Hardy et al. 1975), which may result in more effective hydrogen delivery to high-latitude regions. In addition, Earth wind protons at energies other than 1 keV may contribute to OH/H_2O formation. Protons at higher energies can produce more vacancies, e.g., a 30 keV proton generates about eight vacancies per incident ion (Fink et al. 1995), which can trap more hydrogen to form OH/H_2O, while the 1 keV protons dominant in solar wind can only create about two vacancies per ion (Farrell et al. 2017). Meanwhile, high energy protons can produce deeper vacancy sites (Djouadi et al. 2011), which may hinder their diffusive loss. On the other hand, protons at energies lower than 1 keV are expected to be trapped more easily by vacancies. This is because the ion-solid collision cross-section (which describes the probability of transferring energy from ions to a solid), is inversely proportional to the square of ion energy
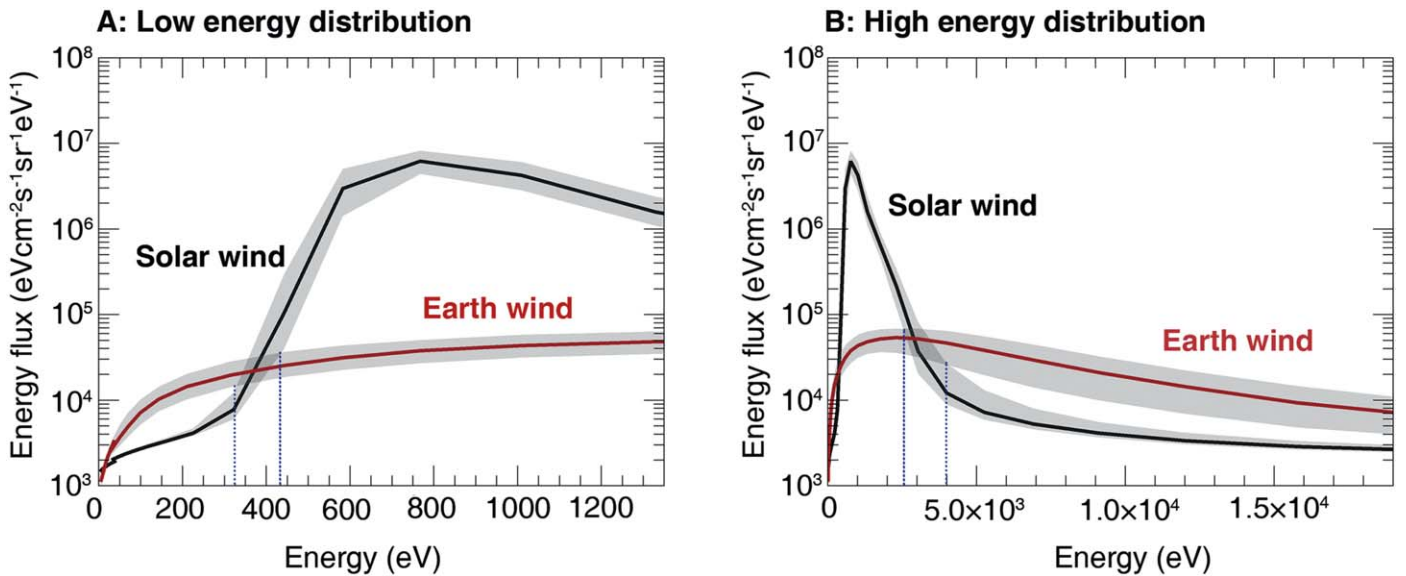
Figure 4. Differential ion energy fluxes for (A) low and (B) high energy ranges in the solar wind and in the magnetosphere, based on averaged 5 yr ARTEMIS ESA data. The two groups of intersection points are around 325–430 eV and 2.5–4 keV. The average differential proton energy fluxes with energy values of less than 325 eV or more than 4 keV are greater in the Earth wind than in solar wind.

(Nastasi et al. 1996). Therefore, even though Earth wind proton energy flux at ∼1 keV is about two orders of magnitude lower than that of solar wind, the protons at the other two energy ranges may provide a more efficient contribution to the formation of OH/H_2O inside the Earth's magnetosphere, which may result in the same level of lunar OH/H_2O abundance inside/outside the Earth's magnetosphere. Thus, this study may give some clues as to the consistency of OH/H_2O abundance at the polar regions over one lunation. Although presently there are no systematic laboratory experiments to study the water production rate over the full energy range covering the solar wind and the Earth wind, Schaible & Baragiola (2014) have shown, at three specific proton energies of 2, 5, and 10 keV, that higher energy protons can produce more water under the same fluence. This suggests that "better" interaction energies than 1 keV may exist, but may or may not be just around the intersection ranges shown in Figure 4, since we should also consider other factors, such as interaction cross-sections. This needs to be studied in future theoretical works, simulations, and laboratory experiments. Another significant difference between the solar wind and Earth wind is the high flux of heavy ions in the Earth wind. These heavy ions, such as oxygen, nitrogen, and hydroxyl ions found in Earth wind might also contribute to the OH/H_2O production process. Terrestrial oxygen ions could flow out primarily from the polar ionosphere, and escape to the magnetosphere (Seki et al. 2001; Zong et al. 2001; Wei et al. 2020). During some special periods, e.g., during geomagnetically active times, the oxygen ion flux could be enhanced, and sometimes even be comparable to the proton flux (Fu et al. 2001). A recent study by the Kaguya spacecraft shows that biogenic terrestrial high energy oxygen ions (1–10 keV) carried by the Earth wind could transport to the Moon and be implanted into the surface of the lunar regolith (Terada et al. 2017). In such a case, oxygen ions in the Earth wind might directly provide oxygen species to the OH/H_2O. In the Earth's upper atmosphere (also that of Mars and some other planets), H_2O molecules can be photodissociated by ultraviolet radiation into atoms and/or hydroxyl ions; and the reverse process i.e., recombination, can also occur (Roble 1995; Fox et al. 2015). At

this time, we cannot conclude whether similar recombination processes take place in the lunar regolith, which is implanted by protons, electrons, and oxygen/hydroxyl ions from the Earth wind. This is an interesting topic for further study. Moreover, irradiation by heavier ions with greater incident energies (Terada et al. 2017) may add multiple vacancies more efficiently, which might hold more implanted protons to form OH/H_2O. To support this possibility, we have carried out some SRIM calculations. The results show that heavy ions can produce more vacancies than protons, e.g., a 1 keV oxygen ion can produce a number of vacancies, one order of magnitude higher than a 1 keV proton. However, the precise mechanism of these processes with different energy/flux and species of ions remain unclear, and more work needs to be done to address this issue.

In a case study, Hendrix et al. (2019) found OH/H_2O abundance to be nearly the same at two different locations inside/outside the Earth's magnetosphere at a mid-latitude region, using Lunar Reconnaissance Orbiter (LRO) Lyman-Alpha Mapping Project (LAMP) data. On the contrary, using the M^3 OP2C data from a statistical study, Li et al. (2018b) suggested that the shielding effect of the Earth's magnetosphere on the formation of the lunar surficial water is pronounced at latitudes 60°–75° S, although this effect is obscured at lower latitudes due to compositional variations in the regolith. From their figures, it appears that the shielding effect of the Earth's magnetosphere tends to be weaker above 65°S; therefore, this does not conflict with our observations at the polar regions. These previous works suggested that the shielding effect is due to a significant and sudden proton flux drop when the Moon enters the Earth's magnetotail, based on the M^3 data (Cho et al. 2018; Li et al. 2018b). However, a decrease in OH/H_2O on the lunar surface was not observed when the Moon was in the Earth's magnetotail (using the LAMP data) and a migration mechanism for the distribution of adsorbed water on the Moon was proposed (Hendrix et al. 2019). It appears that the role of particles from the Earth's magnetosphere has not been considered in these studies, for

example, whether these particles are an important source of global lunar surface hydration.

5. Conclusion and Perspective

In this study, we have presented lunar surficial hydration observations, using the M^3 measurements of Chandrayaan-1, and determined when the Moon was in the magnetotail using Kaguya's MAP data. We find that the probability of lunar OH/H_2O abundance at polar regions when inside the Earth's magnetosphere remains unchanged, as compared to when the Moon is exposed to solar wind, by means of quantitative analysis, while controlling the effects of latitude, composition, and time of day. Possible mechanisms for this unchanged polar surficial hydration while the Moon lies within the Earth's magnetotail have been discussed. We have proposed a possible mechanism with which to interpret the same order of magnitude of lunar hydration inside/outside the Earth's magnetosphere at lower latitude polar regions where the OH/H_2O may not be saturated, whereby the Earth wind (particles from Earth's magnetosphere) can act as an additional source for global lunar hydration, based on both observations and theoretical analysis.

As well as the Chandrayaan-1 M^3 information, the LAMP on board the LRO has obtained a large amount of UV spectral data covering the entire lunar surface from 2009 to the present. This provides an opportunity for comprehensive studies of the spatial distribution and temporal variations of lunar water (Hendrix et al. 2012, 2019), and could provide further evidence in relation to its formation mechanisms. In addition, the Chinese Chang'E-5 lunar sample-return mission is planned to launch in late 2020, and will carry an infrared spectrometer with a spectral range of up to 3.2 μm, which could also help us to study lunar surface water (OH/H_2O). The ARTEMIS mission will concurrently provide accurate and high-resolution plasma data around the Moon, both in the solar wind and in the magnetosphere.

Appendix

Figures A1–A4 show the $OH/H2O$ abundance before/during/after transiting the magnetotail at polar regions, the variation of the longitude ranges with lunar day, data point distribution along with OH/H_2O abundance in the Earth's magnetosphere and in the solar wind, and histogram statistics for OH/H_2O abundance in the Earth's magnetosphere and in the solar wind. Tables A1–A4 list the M^3 data strips we used in the manuscript, quartile values of OH/H_2O abundance at the northern and southern polar regions, mean local time at the northern and southern polar regions varying with lunar day during a lunation from 2009 Jan 26 to 2009 Feb 23, and production/loss processes of the OH/H_2O at high latitudes (70°–85°).
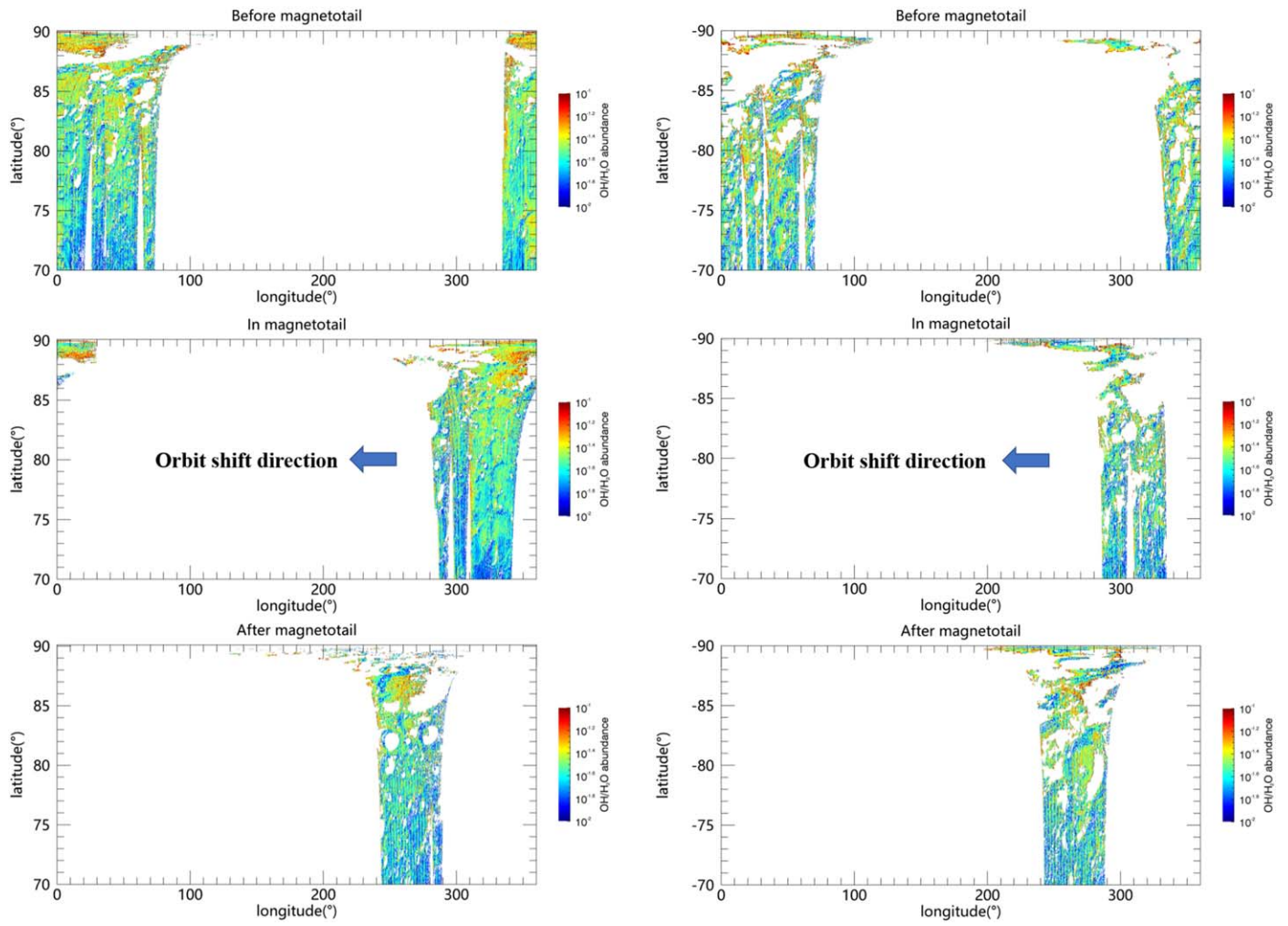
Figure A1. OH/H_2O abundance before/during/after transiting the magnetotail at northern (a)–(c) and southern polar regions (d)–(f). (a) and (d) before magnetotail, (b) and (e) in magnetotail, (c) and (f) after magnetotail.
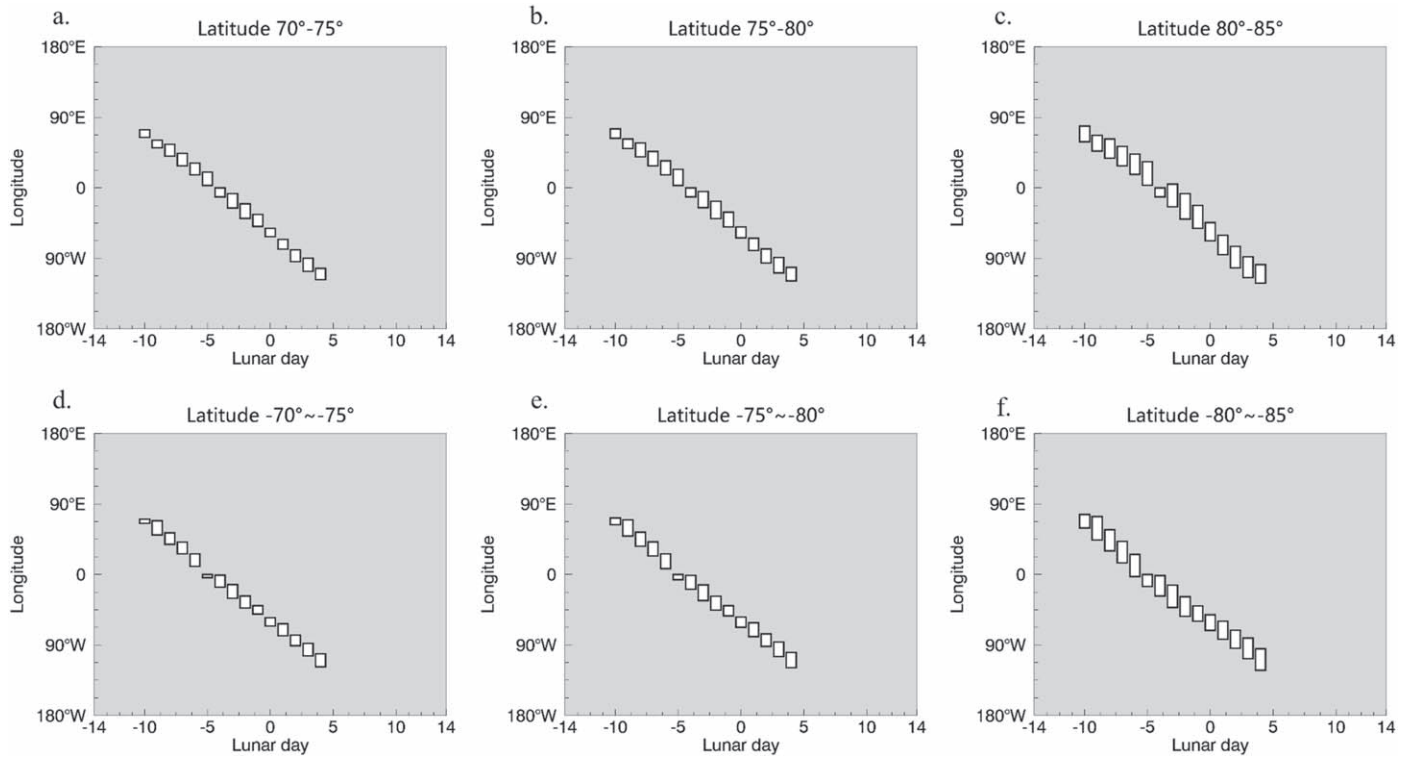
Figure A2. Longitude ranges varying with lunar day at individual latitude ranges (70°–75°, 75°–80°, 80°–85°): (a)–(c) Northern hemisphere; (d)–(f) Southern hemisphere.
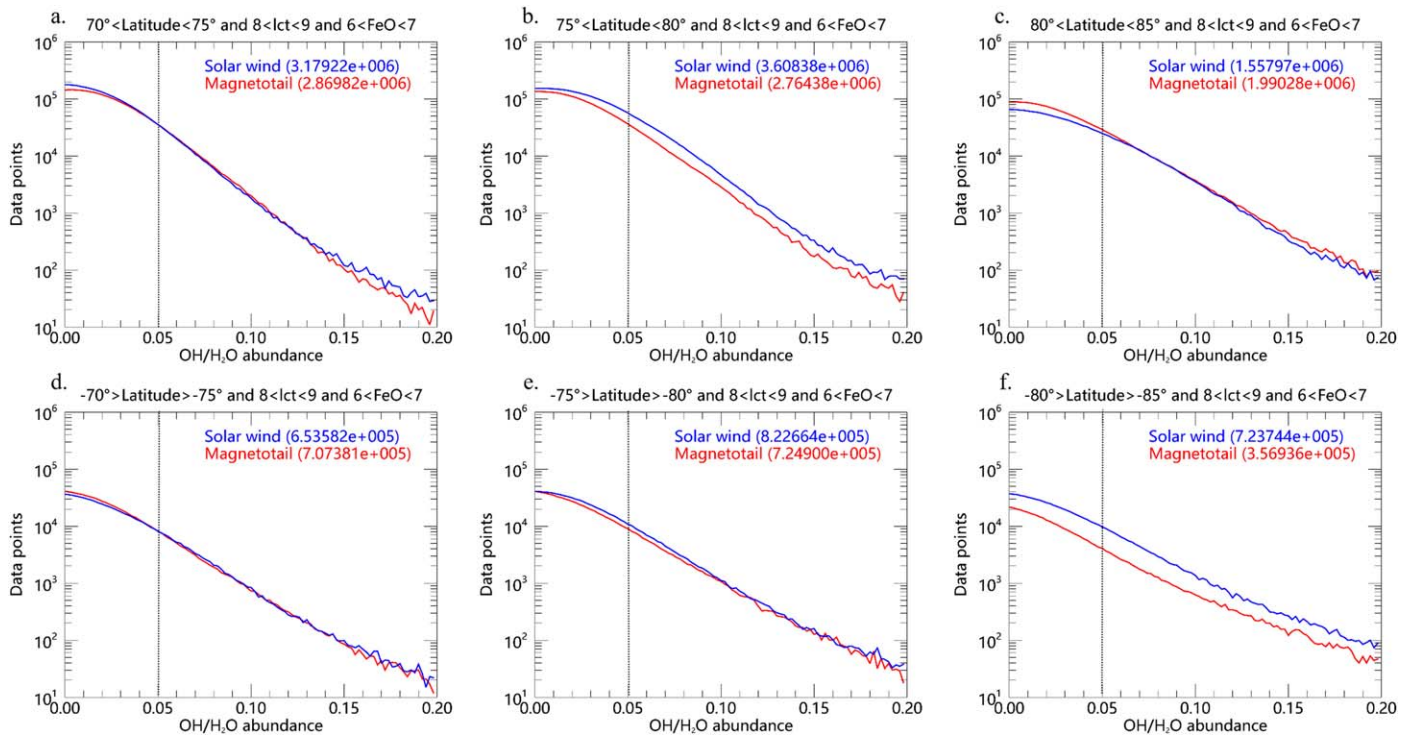
Figure A3. Data point distribution along with OH/H2O abundance in the Earth's magnetosphere (red line) and in the solar wind (blue line) at individual latitude ranges (70°–75°, 75°–80°, 80°–85°) for similar local times (8 am < lct < 9 am) and FeO abundances (6 wt.% < FeO < 7 wt.%) at northern (a)–(c) and southern (d)–(f) polar regions. The number of data points in the solar wind and magnetotail are shown in the upper right of each figure. The black dashed line notes that the absorption depth is 0.05.
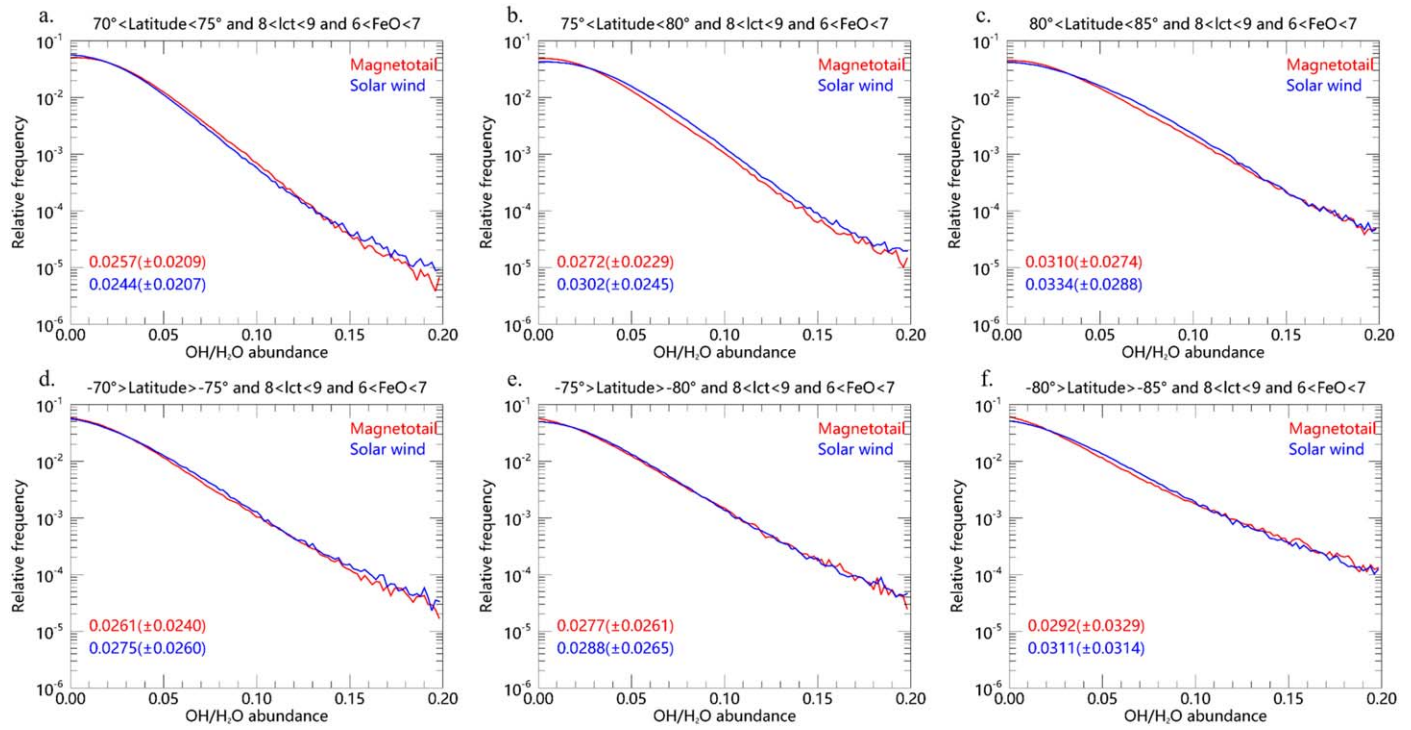
Figure A4. Histogram statistics of OH/H_2O abundance in the Earth's magnetosphere and the solar wind. Results for data at individual latitude ranges (70°–75°, 75°–80°, 80°–85°) for similar local times (8 am < lct < 9 am) and FeO abundances (6 wt.% < FeO < 7 wt.%) at northern (a)–(c) and southern (d)–(f) polar regions. The mean value and standard deviation of the OH/H_2O abundance for an individual latitude range at northern and southern polar regions when in the solar wind (red) and in the magnetotail (blue) are shown.

Table A1
List of the M^3 Data Strips

Data num	Data name	start time	end time	Moon position	Central longitude (°)	Local time (h)	The days before(−)/after(+) the Full moon
1	M3G20090131T051413	2009 Jan 31/05:14:14	2009 Jan 31/05:20:45	Solar wind	71.16	8.92	−9.39
2	M3G20090131T091031	2009 Jan 31/09:10:32	2009 Jan 31/09:16:53	Solar wind	69.19	8.92	−9.23
3	M3G20090131T130631	2009 Jan 31/13:06:31	2009 Jan 31/13:13:00	Solar wind	67.21	8.92	−9.06
4	M3G20090201T064933	2009 Feb 01/06:49:33	2009 Feb 01/06:55:38	Solar wind	58.24	8.92	−8.33
5	M3G20090201T104533	2009 Feb 01/10:45:33	2009 Feb 01/10:51:47	Solar wind	56.21	8.92	−8.17
6	M3G20090201T144133	2009 Feb 01/14:41:33	2009 Feb 01/14:47:58	Solar wind	54.19	8.92	−8.00
7	M3G20090201T163951	2009 Feb 01/16:39:52	2009 Feb 01/16:46:03	Solar wind	53.19	8.92	−7.92
8	M3G20090201T203612	2009 Feb 01/20:36:12	2009 Feb 01/20:42:14	Solar wind	51.19	8.92	−7.75
9	M3G20090202T003211	2009 Feb 02/00:32:11	2009 Feb 02/00:38:24	Solar wind	49.22	8.92	−7.59
10	M3G20090202T042831	2009 Feb 02/04:28:32	2009 Feb 02/04:34:34	Solar wind	47.34	8.93	−7.43
11	M3G20090202T082431	2009 Feb 02/08:24:31	2009 Feb 02/08:30:44	Solar wind	45.54	8.94	−7.26
12	M3G20090202T122051	2009 Feb 02/12:20:51	2009 Feb 02/12:26:53	Solar wind	43.75	8.95	−7.10
13	M3G20090202T161651	2009 Feb 02/16:16:52	2009 Feb 02/16:23:01	Solar wind	41.96	8.97	−6.94
14	M3G20090202T201251	2009 Feb 02/20:12:51	2009 Feb 02/20:19:09	Solar wind	40.16	8.98	−6.78
15	M3G20090203T041059	2009 Feb 03/04:10:59	2009 Feb 03/04:11:23	Solar wind	35.03	8.91	−6.44
16	M3G20090203T080104	2009 Feb 03/08:01:04	2009 Feb 03/08:07:30	Solar wind	34.72	9.02	−6.28
17	M3G20090203T135512	2009 Feb 03/13:55:12	2009 Feb 03/14:01:40	Solar wind	31.91	9.03	−6.03
18	M3G20090203T175131	2009 Feb 03/17:51:31	2009 Feb 03/17:57:46	Solar wind	29.98	9.03	−5.87
19	M3G20090204T113444	2009 Feb 04/11:34:45	2009 Feb 04/11:40:13	Solar wind	20.96	9.03	−5.13
20	M3G20090204T152951	2009 Feb 04/15:29:51	2009 Feb 04/15:36:18	Solar wind	18.76	9.02	−4.97
21	M3G20090204T192552	2009 Feb 04/19:25:52	2009 Feb 04/19:32:24	Solar wind	16.47	9.00	−4.81
22	M3G20090205T031811	2009 Feb 05/03:18:11	2009 Feb 05/03:24:36	Solar wind	11.80	8.95	−4.48
23	M3G20090205T071411	2009 Feb 05/07:14:11	2009 Feb 05/07:20:43	Solar wind	9.47	8.93	−4.31
24	M3G20090205T111013	2009 Feb 05/11:10:13	2009 Feb 05/11:16:50	Solar wind	7.14	8.90	−4.15
25	M3G20090205T150614	2009 Feb 05/15:06:14	2009 Feb 05/15:12:57	Solar wind	4.82	8.88	−3.99
26	M3G20090205T190233	2009 Feb 05/19:02:33	2009 Feb 05/19:09:05	Solar wind	80.73	8.86	−3.82
27	M3G20090205T225833	2009 Feb 05/22:58:33	2009 Feb 05/23:05:13	Solar wind	193.83	8.84	−3.66
28	M3G20090206T025453	2009 Feb 06/02:54:53	2009 Feb 06/03:01:20	Solar wind	282.20	8.83	−3.49
29	M3G20090206T065053	2009 Feb 06/06:50:53	2009 Feb 06/06:57:28	Solar wind	319.05	8.82	−3.33
30	M3G20090206T084850	2009 Feb 06/08:48:50	2009 Feb 06/08:55:32	Solar wind	328.97	8.81	−3.25
31	M3G20090206T124510	2009 Feb 06/12:45:10	2009 Feb 06/12:51:39	Solar wind	340.45	8.80	−3.08
32	M3G20090206T164110	2009 Feb 06/16:41:10	2009 Feb 06/16:47:46	Solar wind	345.63	8.79	−2.92
33	M3G20090206T203710	2009 Feb 06/20:37:10	2009 Feb 06/20:43:53	Solar wind	347.02	8.79	−2.75
34	M3G20090206T222411	2009 Feb 06/22:28:39	2009 Feb 06/22:41:56	Solar wind	346.85	8.78	−2.68
35	M3G20090207T003331	2009 Feb 07/00:33:30	2009 Feb 07/00:39:59	Solar wind	346.25	8.78	−2.59
36	M3G20090207T061610	2009 Feb 07/06:20:50	2009 Feb 07/06:34:08	Solar wind	343.17	8.77	−2.34
37	M3G20090207T082530	2009 Feb 07/08:25:30	2009 Feb 07/08:32:11	magnetotail	342.12	8.76	−2.26
38	M3G20090207T101751	2009 Feb 07/10:22:37	2009 Feb 07/10:35:55	magnetotail	341.06	8.76	−2.18
39	M3G20090207T121011	2009 Feb 07/12:14:56	2009 Feb 07/12:28:17	magnetotail	340.00	8.75	−2.10
40	M3G20090207T142313	2009 Feb 07/14:23:13	2009 Feb 07/14:26:19	magnetotail	337.66	8.66	−2.02
41	M3G20090207T161103	2009 Feb 07/16:11:03	2009 Feb 07/16:24:21	magnetotail	337.78	8.74	−1.94
42	M3G20090207T181550	2009 Feb 07/18:15:50	2009 Feb 07/18:22:23	magnetotail	336.68	8.73	−1.85
43	M3G20090207T200231	2009 Feb 07/20:07:04	2009 Feb 07/20:20:25	magnetotail	335.56	8.72	−1.77
44	M3G20090207T221151	2009 Feb 07/22:11:50	2009 Feb 07/22:18:27	magnetotail	334.45	8.72	−1.69
45	M3G20090207T235830	2009 Feb 08/00:03:09	2009 Feb 08/00:16:30	magnetotail	333.32	8.71	−1.61
46	M3G20090208T020750	2009 Feb 08/02:07:50	2009 Feb 08/02:14:32	magnetotail	332.18	8.70	−1.52

Table A1
(Continued)

Data num	Data name	start time	end time	Moon position	Central longitude (°)	Local time (h)	The days before(−)/after(+) the Full moon
47	M3G20090208T035432	2009 Feb 08/03:59:13	2009 Feb 08/04:12:34	magnetotail	331.04	8.69	−1.44
48	M3G20090208T075032	2009 Feb 08/07:55:17	2009 Feb 08/08:08:38	magnetotail	328.73	8.67	−1.28
49	M3G20090208T100012	2009 Feb 08/10:00:11	2009 Feb 08/10:06:39	magnetotail	327.57	8.65	−1.20
50	M3G20090208T114652	2009 Feb 08/11:51:22	2009 Feb 08/12:04:41	magnetotail	326.41	8.64	−1.12
51	M3G20090208T135610	2009 Feb 08/13:56:10	2009 Feb 08/14:02:43	magnetotail	325.25	8.63	−1.03
52	M3G20090208T154251	2009 Feb 08/15:47:26	2009 Feb 08/16:00:45	magnetotail	324.06	8.62	−0.95
53	M3G20090208T175211	2009 Feb 08/17:52:10	2009 Feb 08/17:58:47	magnetotail	322.90	8.61	−0.87
54	M3G20090208T194335	2009 Feb 08/19:43:35	2009 Feb 08/19:56:49	magnetotail	321.72	8.60	−0.79
55	M3G20090208T214811	2009 Feb 08/21:48:10	2009 Feb 08/21:54:51	magnetotail	320.53	8.58	−0.71
56	M3G20090208T233940	2009 Feb 08/23:39:40	2009 Feb 08/23:52:53	magnetotail	319.32	8.57	−0.62
57	M3G20090209T014431	2009 Feb 09/01:44:30	2009 Feb 09/01:50:55	magnetotail	318.10	8.55	−0.54
58	M3G20090209T033051	2009 Feb 09/03:35:40	2009 Feb 09/03:48:57	magnetotail	316.86	8.54	−0.46
59	M3G20090209T054031	2009 Feb 09/05:40:30	2009 Feb 09/05:46:59	magnetotail	315.60	8.52	−0.38
60	M3G20090209T072710	2009 Feb 09/07:31:45	2009 Feb 09/07:45:01	magnetotail	314.34	8.50	−0.30
61	M3G20090209T212512	2009 Feb 09/21:25:11	2009 Feb 09/21:31:22	magnetotail	305.56	8.38	0.28
62	M3G20090210T012132	2009 Feb 10/01:21:32	2009 Feb 10/01:27:28	magnetotail	303.10	8.35	0.44
63	M3G20090210T051732	2009 Feb 10/05:17:31	2009 Feb 10/05:23:35	magnetotail	300.65	8.32	0.61
64	M3G20090210T210152	2009 Feb 10/21:01:51	2009 Feb 10/21:08:06	magnetotail	291.18	8.22	1.26
65	M3G20090211T005812	2009 Feb 11/00:58:12	2009 Feb 11/01:04:14	magnetotail	288.87	8.20	1.43
66	M3G20090211T045412	2009 Feb 11/04:54:11	2009 Feb 11/05:00:22	magnetotail	286.62	8.18	1.59
67	M3G20090211T085032	2009 Feb 11/08:50:31	2009 Feb 11/08:56:30	solar wind	284.43	8.17	1.75
68	M3G20090211T203852	2009 Feb 11/20:38:51	2009 Feb 11/20:44:49	solar wind	277.62	8.11	2.25
69	M3G20090212T003453	2009 Feb 12/00:34:52	2009 Feb 12/00:40:56	solar wind	275.30	8.09	2.41
70	M3G20090212T043052	2009 Feb 12/04:30:51	2009 Feb 12/04:37:04	solar wind	273.01	8.07	2.57
71	M3G20090212T082712	2009 Feb 12/08:27:11	2009 Feb 12/08:33:11	solar wind	270.83	8.06	2.74
72	M3G20090212T122313	2009 Feb 12/12:23:12	2009 Feb 12/12:29:18	solar wind	268.69	8.05	2.90
73	M3G20090212T162141	2009 Feb 12/16:21:40	2009 Feb 12/16:25:26	solar wind	266.76	8.05	3.06
74	M3G20090212T201532	2009 Feb 12/20:15:31	2009 Feb 12/20:21:33	solar wind	264.45	8.03	3.23
75	M3G20090213T001153	2009 Feb 13/00:11:52	2009 Feb 13/00:17:39	solar wind	262.27	8.01	3.39
76	M3G20090213T040732	2009 Feb 13/04:07:31	2009 Feb 13/04:13:47	solar wind	260.09	8.00	3.56
77	M3G20090213T080353	2009 Feb 13/08:03:51	2009 Feb 13/08:09:54	solar wind	257.96	7.99	3.72
78	M3G20090213T115953	2009 Feb 13/11:59:52	2009 Feb 13/12:06:02	solar wind	255.90	7.99	3.89
79	M3G20090213T155552	2009 Feb 13/15:55:51	2009 Feb 13/16:02:09	solar wind	253.90	7.99	4.05
80	M3G20090213T195213	2009 Feb 13/19:52:11	2009 Feb 13/19:58:16	solar wind	251.93	7.99	4.22
81	M3G20090213T234813	2009 Feb 13/23:48:12	2009 Feb 13/23:54:22	solar wind	249.95	7.99	4.38
82	M3G20090214T013412	2009 Feb 14/01:39:09	2009 Feb 14/01:52:26	solar wind	248.96	7.99	4.46
83	M3G20090214T034413	2009 Feb 14/03:44:12	2009 Feb 14/03:50:29	solar wind	247.97	7.99	4.54
84	M3G20090214T074247	2009 Feb 14/07:42:46	2009 Feb 14/07:46:35	solar wind	246.05	7.99	4.71

Note. The "Data num" is the number of M^3 observations used in this work. The "Data name" is the product ID of the M^3 instrument, which is named based on the start time of each observation, and "G" means lower-resolution global mode data. The start time and end time indicate the M^3 observation time duration we selected according to the latitude. Given that the magnetopause is not as stable as modeled, we use the magnetic field and plasma data from Kaguya in this lunation to determine whether the locations were in the solar wind or in Earth's magnetotail.

Table A2
Quartile Values of OH/H_2O Abundance at Northern and Southern Polar Regions

		Latitude 70°–75°		Latitude 75°–80°		Latitude 80°–85°	
		Solar wind	Earth wind	Solar wind	Earth wind	Solar wind	Earth wind
North polar	25% percentile	0.00918	0.0101	0.0120	0.0104	0.0123	0.0114
	50% percentile	0.0197	0.0211	0.0249	0.0220	0.0266	0.0242
	75% percentile	0.0342	0.0361	0.0424	0.0380	0.0471	0.0429
South polar	25% percentile	0.00945	0.00909	0.0104	0.00947	0.0103	0.00884
	50% percentile	0.0210	0.0199	0.0224	0.0209	0.0229	0.0201
	75% percentile	0.0382	0.0360	0.0398	0.0383	0.0422	0.0385

Table A3
Mean Local Time at Lunar Northern and Southern Polar Regions Varying with Lunar Day During a Lunation from 2009 January 26 to 2009 February 23
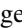
Lunar day	70°N–75°N	75°N–80°N	80°N–85°N	70°S–75°S	75°S–80°S	80°S–85°S
−10	8.93	8.92	8.91	8.93	8.93	8.93
−9	8.90	8.92	8.94	8.87	8.86	8.83
−8	8.90	8.92	8.97	8.79	8.76	8.70
−7	8.91	8.97	9.10	8.69	8.63	8.46
−6	8.91	8.99	9.19	8.55	8.46	8.26
−5	8.84	8.92	9.11	8.46	8.38	8.19
−4	8.73	8.80	8.97	8.41	8.34	8.17
−3	8.63	8.73	8.91	8.32	8.24	8.05
−2	8.59	8.68	8.85	8.26	8.18	8.00
−1	8.49	8.54	8.68	8.25	8.19	8.06
0	8.33	8.34	8.37	8.27	8.26	8.23
1	8.21	8.19	8.17	8.25	8.26	8.28
2	8.11	8.08	8.03	8.21	8.23	8.27
3	8.05	8.02	7.96	8.15	8.17	8.22
4	8.01	8.00	7.97	8.05	8.06	8.07

Table A4
Production/Loss Processes of OH/H_2O Abundance at High Latitudes (70°–85°)

	Process	Concentration	Production/Loss Rate (H_2O/m^2 s)	Mass Flux (g cm^{-2}s^{-1})	Production/Loss Ratio	Condition	References	Remarks on the Processes Involved in This Study
Production	Solar wind	750 ppm	⋯	⋯	⋯	latitude 70°, regolith density 1.7 g cm^{-3}, implantation depth 20 nm;	(Tucker et al. 2019)	Consider to be the main source in the Solar wind in this paper
Loss	Recombination desorption	⋯	⋯	⋯	0	Latitude 75°–90°	(Jones et al. 2018)	Recombination desorption to be irrelevant due to the low temperature in polar region
	Thermal diffusion	⋯	⋯	⋯	64%	$T = 280$ K, $\Delta t = 3.8$ days, $D_0 = 10^{-12}$m^2 s^{-1}	(Farrell et al. 2017)	Consider to be the main loss process in this paper
	sputtering	⋯	8×10^7	⋯	⋯	1 keV proton flux 2×10^{10} protons m^{-2} s^{-1}	(Farrell et al. 2019)	water loss via temperature-dependent process is faster than the plasma and impact environmental loss rate above ∼104 K (Farrell et al. 2019). Thus, in the discussion, we only calculate the thermal diffusion loss rate.
	Photodesorption	⋯	2.7×10^{12}	⋯	⋯	Bullialdus Crater, >8 eV photon flux 10^{12}photons cm^{-2} s	(DeSimone & Orlando 2015)	
		⋯	1.6×10^{12}	⋯	⋯	Gladstone Crater, >8 eV photon flux 10^{12} photons cm^{-2} s	(DeSimone & Orlando 2014)	
	Meteoroid impact (Impact ejecta and vaporization)	⋯	⋯	$(1.3 \sim 3.2) \times 10^{-17}$	⋯	Temperature 500–5000 K	(Benna et al. 2019)	
		⋯	10^{10}	⋯	⋯	Release temperature 4000 K	(Farrell et al. 2019)	

Note. Note that this is not available in previous works.

ORCID iDs

J. Zhang https://orcid.org/0000-0002-8369-871X
Q. Q. Shi https://orcid.org/0000-0001-6835-4751
A. W. Degeling https://orcid.org/0000-0001-7338-9270
I. J. Rae https://orcid.org/0000-0002-2637-4786
Y. Wei https://orcid.org/0000-0001-7183-0229
J. Liu https://orcid.org/0000-0001-6648-8908
A. M. Tian https://orcid.org/0000-0002-4351-551X
W. J. Sun https://orcid.org/0000-0001-5260-658X
J. Chen https://orcid.org/0000-0003-3759-0254
S. T. Yao https://orcid.org/0000-0002-6059-2963
H. Zhang https://orcid.org/0000-0002-3680-4989
L. D. Xia https://orcid.org/0000-0001-8938-1038

References

Acton, C. H. 1996, Nonlinear Mathematics and its Applications (Cambridge: Cambridge Univ. Press)
Angelopoulos, V. 2011, SSRv, 165, 3
Arnold, J. R. 1979, JGR, 84, 5659
Bandfield, J. L., Poston, M. J., Klima, R. L., & Edwards, C. S. 2018, NatGe, 11, 173
Barghouty, A. F. F. W., Meyer, P. R., & Harris, J. H. A., Jr. 2011, NIMPB, 269, 1310
Barnes, J. J., Kring, D. A., Tartèse, R., et al. 2016, NatCo, 7, 11684
Benna, M., Hurley, D. M., Stubbs, T. J., Mahaffy, P. R., & Elphic, R. C. 2019, NatGe, 12, 333
Blanford, G., Borgesen, P., Moeller, W., Maurette, M., & Monart, B. 1985, in Lunar Bases and Space Activities of the 21st Century, ed. W. W. Mendell (Houston, TX: LPI), 603
Boardman, J. W., Pieters, C. M., Green, R. O., et al. 2011, JGRE, 116, E00G14
Boyce, J. W., Liu, Y., Rossman, G. R., et al. 2010, Natur, 466, 466
Cheek, L. C., Pieters, C. M., Boardman, J. W., et al. 2011, JGRE, 116, E00G02
Cho, E., Yi, Y., Yu, J., Hong, I., & Choi, Y. 2018, JGRE, 123, 2110
Christon, S. P., Gloeckler, G., Williams, D. J., et al. 1994, GeoRL, 21, 3023
Clark, R. N. 2009, Sci, 326, 562
Colaprete, A., Schultz, P., Heldmann, J., et al. 2010, Sci, 330, 463
Daly, R. T., & Schultz, P. H. 2018, SciA, 4, r2632
DeSimone, A. J., & Orlando, T. M. 2014, JGRE, 119, 884
DeSimone, A. J., & Orlando, T. M. 2015, Icar, 255, 44
Djouadi, Z., Robert, F., LeSergeant, L., et al. 2011, A&A, 531, A96
Farrell, W. M., Hurley, D. M., Esposito, V. J., McLain, J. L., & Zimmerman, M. I. 2017, JGRE, 122, 269
Farrell, W. M., Hurley, D. M., Hodges, R. R., et al. 2013, P&SS, 89, 15
Farrell, W. M., Hurley, D. M., Poston, M. J., et al. 2019, GeoRL, 46, 8680
Farrell, W. M., Hurley, D. M., & Zimmerman, M. I. 2015, Icar, 255, 116
Feldman, W. C., Maurice, S., Lawrence, D. J., et al. 2001, JGR, 106, 23231
Fink, D., Krauser, J., Nagengast, D., et al. 1995, ApPhA, 61, 381
Fox, J. L., Benna, M., Mahaffy, P. R., & Jakosky, B. M. 2015, GeoRL, 42, 8977
Fu, S. Y., Zong, Q. G., Wilken, B., & Pu, Z. Y. 2001, SSRv, 95, 539
Gladstone, G. R., Randall, H. D. M., Retherford, K. D., et al. 2010, Sci, 330, 472
Greenwood, J. P., Itoh, S., Sakamoto, N., et al. 2011, NatGe, 4, 79
Harada, Y., Futaana, Y., Barabash, S., et al. 2014, JGRA, 119, 3573
Hardy, D. A., Hills, H. K., & Freeman, J. W. 1975, GeoRL, 2, 169
Hasegawa, H., Fujimoto, M., Phan, T.-D., et al. 2004, Natur, 430, 755
Hauri, E. H., Weinreich, T., Saal, A. E., Rutherford, M. C., & Van Orman, J. A. 2011, Sci, 333, 213
Hemingway, D. J., Garrick-Bethell, I., & Kreslavsky, M. A. 2015, Icar, 261, 66
Hendrix, A. R., Hurley, D. M., Farrell, W. M., et al. 2019, GeoRL, 46, 2417
Hendrix, A. R., Retherford, K. D., Randall, G. C., et al. 2012, JGRE, 117, E12001

Hui, H., Peslier, A. H., Zhang, Y., & Neal, C. R. 2013, NatGe, 6, 177
Hundhausen, J. A. 1970, RvGeo, 8, 729
Hurley, D. M., Cook, J. C., Retherford, K. D., et al. 2017, Icar, 283, 31
Ichimura, A. S., Zent, A. P., Quinn, R. C., Sanchez, M. R., & Taylor, L. A. 2012, E&PSL, 345, 90
Jones, B. M., Aleksandrov, A., Hibbitts, K., Dyar, M. D., & Orlando, T. M. 2018, GeoRL, 45, 910
Kasper, J. C., Stevens, M. L., Lazarus, A. J., Steinberg, J. T., & Ogilvie, K. W. 2007, ApJ, 660, 901
Keays, R. R., Ganapathy, R., Laul, J. C., et al. 1970, Sci, 167, 490
Keller, L. P., & McKay, D. S. 1997, GeCoA, 61, 2331
Kramer, G. Y., Besse, S., Dhingra, D., et al. 2011, JGRE, 116, E00G18
Langevin, Y., & Arnold, J. R. 1977, AREPS, 5, 449
Lawrence, D. J., Feldman, W. C., Elphic, R. C., et al. 2002, JGRE, 107, 5130
Li, S., & Garrick-Bethell, I. 2019, GeoRL, 46, 14318
Li, S., Lucey, P. G., Milliken, R. E., et al. 2018a, PNAS, 115, 8907
Li, S., Lucey, P. G., & Orlando, T. M. 2018b, The Shielding Effect of Earth's Magnetotail on the Formation of Lunar Surface Water(OH/H$_2$O) (Texas: The Woodlands)
Li, S., & Milliken, R. E. 2016, JGRE, 121, 2081
Li, S., & Milliken, R. E. 2017, SciA, 3, e1701471
Lin, R. P., Anderson, K. A., Ashford, S., et al. 1995, SSRv, 71, 125
Liu, Y., Guan, Y., Zhang, Y., et al. 2012, NatGe, 5, 779
Livengood, T. A., Chin, G., Sagdeev, R. V., et al. 2015, Icar, 255, 100
Lucey, P. G. 2009, Elements, 5, 41
McCord, T. B., Taylor, L. A., Combe, J. P., et al. 2011, JGRE, 116, E00G05
McCubbin, F. M., Steele, J. A., Hauri, E. H., et al. 2010, PNAS, 107, 11223
McFadden, J. P., Carlson, C. W., Larson, D., et al. 2008, SSRv, 141, 277
Milliken, R. E., & Li, S. 2017, NatGe, 10, 561
Nastasi, M., Mayer, J. W., & Hirvonen, J. K. 1996, Ion–Solid Interactions: Fundamentals and Applications (Cambridge: Cambridge Univ. Press)
Pieters, C. M., Goswami, J. N., Clark, R. N., et al. 2009, Sci, 326, 568
Poppe, A. R., Fillingim, M. O., Halekas, J. S., Raeder, J., & Angelopoulos, V. 2016, GeoRL, 43, 6749
Roble, R. G. 1995, in The Upper Mesosphere and Lower Thermosphere: A Review of Experiment and Theory, Geophysical Monograph Series, Vol. 87, ed. R. M. Johnson & T. L. Killeen (Washington, DC: AGU), 1
Saal, A. E., Hauri, E. H., Lo Cascio, M., et al. 2008, Natur, 454, 192
Saal, A. E., Hauri, E. H., Van Orman, J. A., & Rutherford, M. J. 2013, Sci, 340, 1317
Saito, Y., Yokota, S., Asamura, K., et al. 2008, EP&S, 60, 375
Saito, Y., Yokota, S., Asamura, K., et al. 2010, SSRv, 154, 265
Schaible, M. J., & Baragiola, R. A. 2014, JGRE, 119, 2017
Seki, K., Elphic, R. C., Hirahara, M., Terasawa, T., & Mukai, T. 2001, Sci, 291, 1939
Shang, W. S., Tang, B. B., Shi, Q. Q., et al. 2020, JGRA, 125, e27401
Shi, Q. Q., Zong, Q.-G., Fu, S. Y., et al. 2013, NatCo, 4, 1466
Sibeck, D. G., Angelopoulos, V., Brain, D. A., et al. 2011, SSRv, 165, 59
Starukhina, L. 2001, JGRE, 106, 14701
Starukhina, L. 2012, Water on the Moon: What is Derived from the Observations? (Berlin: Springer)
Starukhina, L., & Shkuratov, Y. G. 2000, Icar, 147, 585
Sunshine, J. M., Farnham, T. L., Feaga, L. M., et al. 2009, Sci, 326, 565
Terada, K., Yokota, S., Saito, Y., et al. 2017, NatAs, 1, 26
Tsunakawa, H., Shibuya, H., Takahashi, F., et al. 2010, SSRv, 154, 219
Tucker, O. J., Farrell, W. M., Killen, R. M., & Hurley, D. M. 2019, JGRE, 124, 278
Watson, K., Murray, B. C., & Brown, H. 1961, JGR, 66, 3033
Wei, Y., Pu, Z., Zong, Q., et al. 2014, E&PSL, 394, 94
Wei, Y., Zhong, J., Hui, H., et al. 2020, GeoRL, 47, e86208
Wöhler, C., Grumpe, A., Berezhnoy, A. A., & Shevchenko, V. V. 2017, SciA, 3, e1701286
Zeller, E. J., Ronca, L. B., & Levy, P. W. 1966, JGR, 71, 4855
Zhu, C., Crandall, P. B., Gillis-Davis, J. J., et al. 2019, PNAS, 116, 11165
Zong, Q. G., Wilken, B., Fu, S. Y., et al. 2001, JGR, 106, 25541